ROYAL SOCIETY OF CHEMISTRY

Journal Name

ARTICLE

Structural transformation of metal-organic framework MIL-68(Al) to obtain nanosheets of MIL-53(Al) applied in membranes with improved CO_2/N_2 and CO_2/CH_4 selectivities

Adelaida Perea-Cachero,[a] Javier Sánchez-Laínez,[a] Beatriz Zornoza,[a] Enrique Romero-Pascual,[b] Carlos Téllez[a] and Joaquín Coronas[a,†]

MIL-68(Al) and MIL-53(Al) are carboxylate-based metal-organic frameworks (MOFs) with the same chemical composition but different structures (polymorphs). In this study, the structural transformation from MIL-68(Al) to MIL-53(Al) was carried out by immersion in water under different conditions (ultrasound, stirring, reflux, 60 °C and room temperature) following a crackling core model. The transformation process gave rise to MIL-53(Al) nanosheets of ca. 150 nm in size with an average thickness of 3.5 ± 0.9 nm. The disaggregated MIL-53(Al) nanosheets prepared under the more severe conditions were suspended in a PDMS solution and then deposited on asymmetric polyimide P84® supports under vacuum filtration to form supported mixed matrix membranes (MMMs). When applied to the separation of CO_2/CH_4 and CO_2/N_2 mixtures, the MMM with MIL-53(Al) nanosheets improved the CO_2/CH_4 (28.4-28.7 vs. 22.4) and CO_2/N_2 (19.9-23.2 vs. 17.5) selectivities of the conventional MIL-53(Al) MMM with higher CO_2 permeances (20.8-29.6 GPU vs. 9.5 GPU for CO_2/CH_4 and 17.7-26.8 GPU vs. 11.2 GPU for CO_2/N_2).

Introduction

Metal-organic frameworks (MOFs) are constructed by the coordination of metallic ions or clusters through organic ligands giving porous structures in one, two or three dimensions (1D, 2D or 3D).[1] MOFs have remarkable properties such as large pore volumes and surface areas, excellent thermal and chemical stabilities, structural flexibility,[2] a wide range of pore sizes,[3] and framework diversity.[4] The shape, size and chemical surface of the pores and the properties of the MOF can be tuned by using the appropriate organic and inorganic moieties in the synthesis.[5-7] The large variety of metals and organic molecules and the possibility of post-functionalization could result in an unlimited number of different hybrid frameworks with distinct features.[5-7] As a consequence, MOFs have been studied in several applications such as catalysis,[8, 9] gas separation[10] and storage,[8, 11] adsorption,[12] encapsulation,[13] drug delivery,[8] and water treatment.[14]

MILs (Matériaux de l'Institut Lavoisier) constitute a subfamily of MOFs. They are commonly built by trivalent metal cations (Al^{3+}, Cr^{3+}, $V^{3+/4+}$, Fe^{3+}, Sc^{3+}, In^{3+}) and carboxylate-type ligands to originate highly porous and moisture stable frameworks.[15] MIL-53 and MIL-68 are two of the most well-known MIL type materials. They are strongly correlated because MIL-53 and MIL-68 are polymorphs (structural,[16] topological[17, 18] or framework[19] isomers) when activated, i.e. when they do not contain guest molecules inside the pores.[20] MIL-68 and MIL-53 are composed of infinite trans chains of inorganic $MO_4(OH)_2$ octahedra sharing the hydroxyl groups which are sited at apical positions.[5, 21] These inorganic chains are connected through terephthalate anions defining diamond-shaped channels in MIL-53 (Fig. 1a) and triangular as well as hexagonal tunnels in MIL-68 (Fig. 1b).[5, 21, 22] MIL-53 exhibits the so-called breathing effect in which the host framework adapts its pore opening to accommodate guest molecules without crystallinity loss or bond breaking.[23] Thus, the size of the one-dimensional pores in MIL-53 depends on the nature of the adsorbed guest molecules.[24] The MIL-53(Al) structure contains disordered terephthalic acid molecules inside the pores after its synthesis, forming MIL-53(Al)as (as-synthesized).[24] When activated, the terephthalic acid is removed from the pores giving the MIL-53(Al)lp (large-pore or high-temperature, ht) form with empty and open pores.[24] Upon exposure to the environment, the MOF adsorbs water molecules which establish interactions with the pore walls producing the MIL-53(Al)np (narrow-pore or low-temperature, lt) phase with shrunken pores.[24] The high thermal stability of both MIL-53 and MIL-68 materials based on Al^{3+} along with the flexibility of MIL-53 have prompted their use in different fields, such as isomer separation,[25] chemical sensing,[26] gas adsorption[27] and separation,[28] organic solvent

a. Chemical and Environmental Engineering Department and Instituto de Nanociencia de Aragón (INA), Universidad de Zaragoza, 50018 Zaragoza, Spain
b. Chemical and Environmental Engineering Department and Aragón Institute of Engineering Research (I3A), Universidad de Zaragoza, 50018 Zaragoza, Spain
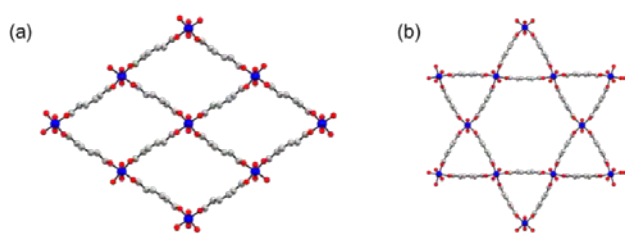† Corresponding author: coronas@unizar.es

ARTICLE

Fig. 1. Unidimensional pore systems of (a) MIL-53as (CCDC 220475)24 (along the b axis) and (b) MIL-6833 (along the c axis). Metal, O and C atoms are coloured in blue, red and grey, respectively. Terephthalic acid and guest molecules from MIL-53as and MIL-68, respectively, and H atoms are omitted for clarity.

nanofiltration[29, 30] and the removal of hazardous contaminants.[31, 32]

Membranes have arisen as an attractive alternative replacing conventional gas separation methods due to their smaller carbon footprint, lower costs, energy savings, ease of processing and reliability.[2, 34] Currently, polymeric membranes dominate commercial gas separations owing to their low cost, processability and mechanical stability.[2] However, they present a trade-off between permeability and selectivity, besides poor chemical and thermal stability and short lifetimes.[2] Inorganic membranes have high selectivities along with high chemical and thermal stabilities, but this kind of membrane suffers from high production costs, limited ranges of pore size and restricted chemical tailorability.[2, 34] Mixed matrix membranes (MMMs) appear to combine the advantages of both polymeric and inorganic materials, such as high gas permeation flows and selectivities.[2, 34] In MMMs, porous inorganic particles (fillers) are dispersed in a polymeric matrix to create a hybrid composite membrane. Silica, carbon molecular sieves and zeolites have been widely used as fillers, but MOFs have attracted special attention in recent years due to their better compatibility with polymers and easy tuning of pore sizes and adsorption properties.[35]

Crystalline-state transformations are reactions where a single crystal or a polycrystalline-constituted solid phase is transformed into another solid phase after an external stimulus (e.g. temperature, pressure, removal or exchange of guest molecules, light, heat and post-synthetic modification) without damage in the ordering of the lattice.[36] Crystals and host frameworks change their chemical compositions and structures upon topology alterations and skeleton distortions.[37] Crystalline-state transformations also include changes in the species or in the amount of adsorbed guest molecules producing different chemical compositions of the crystals without suffering a chemical reaction.[37] Drastic structural changes usually modify the size, morphology, transparency and colour of crystals.[38, 39] The following examples illustrate some crystalline transformations involving MIL type materials. The MOFs MIL-101(V) and MIL-88B(V) underwent framework isomerism to MIL-47 when heated at 200 °C in ethanol or in an ethanol/HCl mixture, respectively.[40] Stavitski *et al*. reported the formation of NH₂-MIL-101(Al) from the crystal growth of NH₂-MOF-235 in N,N-dimethylformamide (DMF) (containing Al^{3+} and terephthalate ions) as the temperature rose.[41] Choi *et al*. found

that MIL-68(In) suffered a structural and morphological transformation to QMOF-2 when immersed in water at 100 °C with an excess amount of terephthalic acid.[42] The hexagonal lumps of Kagomé-like MIL-68(In) were transformed into pointed hexagonal rods of quartz-structured QMOF-2. The encapsulation and release of caffeine produced a reversible transformation involving the NH₂-MIL-88B(Fe) structure. Besides, NH₂-MIL-53(Fe) turned into NH₂-MIL-88B(Fe) when it was activated in ethanol.[43] Finally, Perea-Cachero et al. have recently speculated on the transformation of MIL-53(Al) to MIL-68(Al)[44] (or the MIL-53(Al)DMF, as claimed later by Kriesten et al.[45]).

In this work, the transformation from MIL-68 to delaminated MIL-53 using Al^{3+} as a metallic cation is reported. The immersion of as-made MIL-68(Al) in water under different conditions provoked a transition towards the MIL-53(Al)as structure, and its subsequent delamination. The obtained 2D MIL-53(Al) crystals (nanosheets) of the intermediate products were employed to fabricate supported mixed matrix membranes for gas separation. The membranes were applied in the CO_2 separation from CO_2/N_2 and CO_2/CH_4 mixtures, typical of post-combustion and natural gas purification processes, respectively. As well as zeolites,[46] certain 2D MOFs (with less hydrothermal stability than MIL-53(Al))[47] have been shown to have the potential to create highly efficient membranes for gas separation.[48] To the best of our knowledge, this is the first time that MIL-53(Al) nanosheets have been produced.

Experimental

General methods and materials

Aluminium chloride hexahydrate ($AlCl_3 \cdot 6H_2O$, 99 %, Sigma-Aldrich), aluminium nitrate nonahydrate ($Al(NO_3)_3 \cdot 9H_2O$, ≥98 %, Sigma-Aldrich), terephthalic acid (H_2BDC, C_6H_4-1,4-$(CO_2H)_2$, 98 %, Aldrich), isopropyl alcohol (IPA, ≥99.5 %, C_3H_8O, Scharlau), dimethyl sulfoxide (DMSO, C_2H_6OS, ≥99.5 %, Scharlau), *N,N*-dimethylformamide (DMF, $HCON(CH_3)_2$, 99.95 %, Scharlau) and n-hexane (C_6H_{14}, ≥95 %, Scharlau) were used as purchased without further purification. Polyimide P84® powder was purchased from HP Polymer GmbH. Poly(dimethylsiloxane) (PDMS, Sylgard® 184) was purchased from Ellsworth Adhesives Ibérica. The Sylgard® 184 silicone elastomer kit comprised two components: a base and a curing agent.

MIL-68(Al) and MIL-53(Al) syntheses

MIL-68(Al) was prepared following the procedure reported by Yang et al.[49] Aluminium chloride hexahydrate (0.488 g) and H_2BDC (0.5 g) were dissolved in DMF (30 mL) inside a round bottom flask. The solution was heated under reflux at 130 °C for 18.5 h. After cooling down, the product was recovered by centrifugation (10,000 rpm for 15 min) and washed 3 times with fresh DMF. Finally, MIL-68(Al)as (as-synthesized) was dried at ambient temperature.

MIL-53(Al) was hydrothermally synthesized under the conditions described by Loiseau et al.[24] Aluminium nitrate nonahydrate (6.5 g) and H_2BDC (1.437 g) were mixed in

Dalton Transactions Accepted Manuscript

ARTICLE

deionized water (25 mL). The suspension was then placed in a Teflon™-lined autoclave. The autoclave was put inside a conventional oven at 220 °C for 3 d. After reaction, MIL-53(Al)as was collected by centrifugation (10,000 rpm for 15 min), rinsed 3 times with deionized water and dried at room temperature. Terephthalic acid was removed from the MIL-53(Al)as pores upon calcination at 330 °C for 3 d with heating and cooling rates of 1 °C min^{-1}. The exposure to ambient conditions produced the MIL-53(Al)np.

Preparation of MIL-53(Al) nanosheets

Three different strategies were developed to attain MIL-53(Al) from MIL-68(Al). MIL-68(Al)as was used as the initial material in all cases. The three procedures are described below starting from the mildest method and finishing with the most severe. A simple nomenclature is adopted in order to name the distinct samples obtained after the conversion process: *A-B-C*. *A* refers to the treatment type (*US* for ultrasound, *ST* for stirring, *REF* for reflux), *B* indicates the temperature (*RT* for room temperature) and *C* designates the treatment length. The first approach consisted of immersing the MIL-68(Al)as sample in water at 60 °C in an ultrasound bath for 45 min (US-60°C-45min). In the second strategy, MIL-68(Al)as was soaked in water under stirring at room temperature for 3, 12 and 30 d (ST-RT-3/12/30d). In the last method, MIL-68(Al)as was suspended in water under reflux and stirring at 60 °C for 14 d (REF-60°C-14d). Finally, the products were collected by centrifugation (10,000 rpm for 15 min) and dried at ambient conditions.

As MIL-53(Al)as, ST-RT-30d and REF-60°C-14d were calcined at 330 °C for 3 d with heating and cooling ramps of 1°C min^{-1}. They were then treated under sonication in n-hexane for 30 min to separate the nanosheets. The products (MIL-53(Al) nanosheets) were dried in an oven at 90 °C overnight giving ST-RT-30d-ns and REF-60°C-14d-ns.

Preparation of membranes on polymeric substrates

Flat asymmetric polyimide supports were formed by a phase inversion procedure from a 20 wt% solution in DMSO. The solution was stirred at room temperature overnight. It was cast onto a glass surface using an Elcometer 4340 Automatic Film Applicator and then immediately soaked in a tap water bath (25 °C) for 10 min. The polyimide support was peeled off, washed in deionized water for 48 h (refreshing the solvent every 24 h) and IPA for 1 h (refreshing the alcohol after 30 min). Finally, it was dried at 100 °C overnight.

A 5 wt% PDMS solution was prepared by mixing the base and the curing agent in a 10:1 weight ratio in n-hexane. The membranes were fabricated with MIL-53(Al)np and the disaggregated nanosheets ST-RT-30d-ns and REF-60°C-14d-ns. A suspension was prepared by dispersing ca. 5 mg of one of the above three materials in 2 mL of PDMS solution in an ultrasound bath (5 min). It was stirred at room temperature until it was used. Polyimide supports, 4.9 cm^2 in circular area, were cut from the polymeric sheet. As a previous stage to the membrane fabrication, the support was immersed in the PDMS solution twice for 10 min, allowing the solvent to evaporate between immersions. The support was put in a polycarbonate filter holder (25 mm in diameter, Sartorius Stedim Biotech GmbH) and the sample suspension was added and vacuum filtered through the polyimide support overnight. For the membrane without sample loading (bare membrane), 2 mL of PDMS solution was used instead. The membranes were dried at room temperature for 2 h and at 100 °C for 24 h to give MIL-53(Al)np_m, ST-RT-30d-ns_m and REF-60°C-14d-ns_m (_*m* refers to a membrane sample). Nanosheet agglomeration was studied by preparing suspensions of ST-RT-30d-ns and REF-60°C-14d-ns in ethanol (Fig. S1).

Characterization

Fourier transform infrared (FTIR, Shimadzu IRAffinity-1) spectroscopy was used to evaluate the chemical structure of the intermediate products by means of the KBr disk technique in the 4000-400 cm^{-1} wavenumber range, with a resolution of 4 cm^{-1} and an average of 20 scans. The chemical structure of the membranes was analysed by attenuated total reflectance Fourier transform infrared (ATR-FTIR, Bruker Vertex 70 FTIR) spectroscopy, recording the spectra between 4000 and 600 cm^{-1} with an accuracy of 4 cm^{-1} and an average of 40 scans.

The chemical structure of the intermediate products was also examined by means of solid-state nuclear magnetic resonance (NMR, Bruker Avance III WB400) spectroscopy. NMR spectra were recorded with 4 mm zirconia rotors spun at the magic angle in N$_2$ at 12 kHz. Conventional ^{13}C cross-polarization magic angle spinning (CP-MAS) NMR spectra were acquired with a ^{1}H π/2 pulse length of 3.0 μs, a contact pulse of 3 ms (ramped for ^{1}H) and a recycle delay of 10 s. During the acquisition period of the ^{13}C CP-MAS spectra, an ^{1}H 64-step small-phase incremental alternation (SPINAL-64) decoupling sequence was implemented with a pulse length of 5.3 μs. A total of 1024 scans were collected for each spectrum. The spectrometer operated at 100.6 MHz.

Thermogravimetric analyses (TGA, Mettler Toledo TGA/DSC 1 SF/755) of bulk powder and membranes were carried out to study the stability of the samples and the presence of guests. TGA characterization was performed from 25 to 900 °C in air atmosphere with a heating rate of 5 °C min^{-1}.

Structural changes in the intermediate products and membranes were examined through powder X-ray diffraction (PXRD, D-Max Rigaku and Bruker D8 Advance). Patterns were collected at room temperature with a copper anode using a graphite monochromator to select CuKα radiation with λ = 0.15418 nm. Molecular graphics of MIL-53 and MIL-68 were made with Diamond[50] software from the cif files of MIL-53(Al)as (CCDC 220475)[24] and MIL-68(Sc),[33] respectively.

The morphology of the intermediate products and membranes was explored by scanning electron microscopy (SEM, FEI Inspect F50), taking images in the voltage range of 15-20 kV. Specimens were coated with platinum. To study the cross-section of membranes by SEM, small pieces were broken inside a liquid N$_2$ bath (freeze-fracturing) to achieve clean cross-sectional surfaces. The thicknesses of the MMMs were measured from cross-sectional SEM images with ImageJ[51] software as the

average of at least 15 measurements taken from three or more images. Composition lines across the sections of the membranes were analysed by energy-dispersive X-ray spectroscopy (EDX) using a Quanta FEG-250 SEM microscope.

Transmission electron microscopy (TEM, FEI TECNAI T20) images were acquired at an acceleration voltage of 200 kV. Powder samples (ca. 1 mg) were dispersed in 5 mL of ethanol in an ultrasonic bath for 5 min. A drop of the suspension was poured onto a carbon-coated copper grid (200 mesh), allowing the solvent to evaporate at room temperature. The ImageJ[51] software was also employed to determine the dimensions of the MIL-53(Al) nanosheets from TEM images. The side dimensions and thicknesses were estimated doing at least 5 measurements.

N_2 physisorption isotherms of the intermediate products, MIL-68(Al) and MIL-53(Al) were measured at -196 °C (Micromeritics Tristar 3000 porosity analyser). Sorption data were employed to calculate Brunauer-Emmett-Teller (BET) specific surface areas and t-plot external specific areas. In the t-plot method, the thickness of adsorbed multi-molecular films was calculated using the Harkins and Jura equation[52] in a thickness range of adsorbed layer (t) between 0.385 and 0.468 nm. Prior to the sorption analyses, MIL-68(Al)as and MIL-53(Al)np samples were evacuated at 260 and 200 °C, respectively, for 8 h with a heating rate of 10 °C min^{-1}. The intermediate products were also outgassed at 260 °C for 8 h with the same heating rate.

Gas separation experiments

The separation performance of the membranes was studied as follows. The membranes, 3.14 cm^2 in area, were supported on a 316LSS macroporous disk inside a stainless steel module and gripped with Viton® O-rings. The macroporous support (Mott Corporation) had a nominal pore size of 20 μm. Experiments were carried out at 35 °C inside an oven to control the temperature. Equimolar CO_2/CH_4 and 10/90 vol% CO_2/N_2 gas mixtures were fed into the module at 3 bar through two mass-flow controllers (Alicat Scientific, MC-100CCM-D) with a total volumetric flow of 50 and 100 cm^3(STP) min^{-1}, respectively. The permeate side was swept at 1 bar with a 1 cm^3(STP) min^{-1} mass-flow controlled stream of He (Alicat Scientific, MC-5CCM-D). An Agilent 3000A online gas microchromatograph equipped with a thermal conductivity detector (TCD) was used to determine the concentration of both gas components in the permeate stream. Measurements were collected after achieving the steady state (around 1.5 h). Permeance values were expressed in GPU units (1 GPU = 10^{-6} cm^3(STP) cm^{-2} s^{-1} cmHg^{-1}). Selectivity, $S_{i/j}$, was calculated as the ratio of the permeability of the component i over that of the component j in the binary gas separation. Since the permeance flows were in line with the sweep was of 1 cm^3 min^{-1}, it was assumed that no concentration polarization occurred.

Results and discussion

Characterization of the intermediate products

As-made MIL-68(Al) was used as the starting material to carry out the transformation into MIL-53(Al) nanosheets. The FTIR spectra of MIL-68(Al)as and MIL-53(Al)as are shown in Fig. S2. Both spectra match quite well, as expected, because they are polymorphs having the same metal cation, ligand and, thus, functional groups. However, there are slight differences in the FTIR spectra of both MOFs that could serve as a medium to distinguish them (see Fig. S2 caption). The band at 1700 cm^{-1} in MIL-53(Al)as corresponds to the carbonyl (C=O) group from the free terephthalic acid trapped in the pores during the synthesis. In MIL-68(Al)as this band could be hidden by a more intense signal placed at 1673 cm^{-1} related to the carbonyl group from the DMF present in its cavities. The spectra for the MIL-68(Al) materials soaked in water under different conditions are also depicted in Fig. S2. The first changes towards MIL-53(Al) were observed after sonication at 60 °C for 45 min (US-60°C-45min). The bands at 3682 and 598 cm^{-1} and within 1336-1218 cm^{-1} and 1054-937 cm^{-1} grew in intensity in all the products, resembling MIL-53(Al)as. The typical DMF band disappeared whereas that of the free terephthalic acid arose, indicating that terephthalic acid molecules were formed during the transformation. The process at 60 °C and 14 d (REF-60°C-14d) led to a spectrum similar to those of the MIL-68(Al) immersed in water for 12 and 30 d (ST-RT-12/30d). The increase in temperature speeded up the transformation, as expected. Despite the visible changes in FTIR spectra towards MIL-53(Al)as, a complete conversion was not achieved, so that the different samples obtained were considered as intermediate products between MIL-68(Al) and MIL-53(Al), as subsequently confirmed by PXRD.

TGA and differential thermogravimetric (DTG) curves of MIL-68(Al)as, MIL-53(Al)as and MIL-53(Al)np in air atmosphere are displayed in Fig. S3. MIL-68(Al)as showed four steps. The weight loss at low temperature (25-60 °C) was due to water elimination (1.7 %) while the loss between 60 and 300 °C was attributed to DMF removal from the triangular pores (23.8 %).[49] The little step of ca. 0.4 % at 300-370 °C was assigned to release of terephthalic acid molecules. The MOF decomposition took place from ca. 430 °C. The thermogram relating to MIL-53(Al)as showed two main weight losses. The first (250-480 °C) was divided into two steps, ascribed to the elimination of free terephthalic acid from the pores. The second event above 480 °C was related to framework decomposition. Concerning MIL-53(Al)np, the dehydration process caused the first loss (below 100 °C; 6.2 %) whereas it decomposed above 480 °C. As can be seen, the thermal stability of MIL-53(Al) exceeds that of MIL-68(Al) at around 50 °C. The MIL-68(Al) products clearly evolved into MIL-53(Al)as over time with all three water treatments (Fig. S3). Unlike MIL-53(Al)as, all the samples underwent a weight loss at low temperature (below 100 °C) corresponding to encapsulated water. DMF molecules mostly disappeared in only 45 min under sonication at 60 °C (US-60°C-45min), as observed by the FTIR spectra. The steps deriving from free terephthalic acid arose and became well-differentiated as the water treatment became more severe and the time increased. The appearance of the weight losses from the free terephthalic acid indicated its formation inside the pores. The degradation of US-60°C-45min, ST-RT-30d and REF-60°C-14d took place above 430

ARTICLE

°C, as that of MIL-68(Al)as. Although the transformation towards MIL-53(Al) is evident, its structure is not totally accomplished in any case. The TGA results thus corroborated those of the FTIR characterization.

MIL-68(Al)as crystals had the shape of needles with a size of around 1.25 μm (Fig. 2a). They were arranged forming spherical aggregates. MIL-53(Al) typically crystallizes as elongated hexagonal prisms[53] (Fig. S4). Nonetheless, the crystals obtained after the synthesis were not completely formed, as observed in Fig. 2b. They were up to 10 μm in size. Morphology studies of the five intermediate products were carried out through SEM (Fig. 2c.1-g.1) as well as TEM (Fig. 2c.2-g.2) characterization. According to the SEM images, the MIL-68(Al)as crystals treated under ultrasound at 60 °C for 45 min (US-60°C-45min, Fig. 2c.1) hardly differed from the as-made MOF crystals (Fig. 2a), although they had round and non-defined edges. When the treatment conditions became more severe, the outer crystals of the aggregates broke into small irregular particles, though it is possible to distinguish sheets less than 150 nm in size in the samples ST-RT-12d and ST-RT-30d (Fig. 2e.1 and 2f.1, respectively). It is clear from the SEM images that ST-RT-12d, ST-RT-30d and REF-60°C-14d (Fig. 2g.1) were formed by submicron size crystals. For all the intermediate products, the TEM images showed that spherical aggregates broke into smaller pieces (Fig. 2c.2-g.2), these pieces being wrapped by the same kind of nanosheets seen in the SEM images of ST-RT-12d and ST-RT-30d. The core of the aggregates seems to have remained intact during the processes followed in the transformation of MIL-68(Al) to MIL-53(Al). The thorough analysis of the TEM images

was useful to establish the nanosheet dimensions. Square nanosheets with sides ranging from 25 to 145 nm were found. The largest nanosheets were observed in US-60°C-45min (ca. 145 x 140 nm) while the smallest ones belonged to ST-RT-12d (25-45 nm in side). ST-RT-30d and REF-60°C-14d had nanosheets with sides between 38 and 90 nm. On the other hand, an average and reliable thickness of 3.5 ± 0.9 nm was measured taking into account the five samples of the intermediate products characterized by TEM.

PXRD curves of MIL-68(Al)as and MIL-53(Al)as are depicted in Fig. 3. MIL-53(Al)as had a high crystallinity when compared to MIL-68(Al)as. Products soaked in water under ultrasound at 60 °C for 45 min (US-60°C-45min) and under stirring for 3 d (ST-RT-3d) were obviously intermediate materials between MIL-68(Al)as and MIL-53(Al)as since the corresponding patterns shared peaks from both frameworks (Fig. 3). Solids in water for 12, 30 and 14 (60 °C) d with stirring or reflux (ST-RT-3/12/30d and REF-60°C-14d) almost accomplished the MIL-53(Al)as structure. In fact, even though all the peaks matched well with those of MIL-53(Al)as, a reflection placed at around 2θ = 8.6° (unknown phase) was visible in US-60°C-45min. The other intermediate products showed the same reflection shifted to 2θ = 8.2°. Its intensity diminished with more severe conditions but it did not vanish completely.

To gain insight into the TEM analysis of one of the intermediate products (REF-60°C-14d), electron diffraction was carried out. Fig. 4e shows the selected area where only MIL-53(Al) nanosheets can be depicted. The diffraction pattern corresponding to the nanosheets evidences the MIL-53(Al) phase, confirming that its crystal structure is intact (*t*=0) (Fig. 4f). In agreement with the PXRD, the reflection peak of 2θ = 8.2°
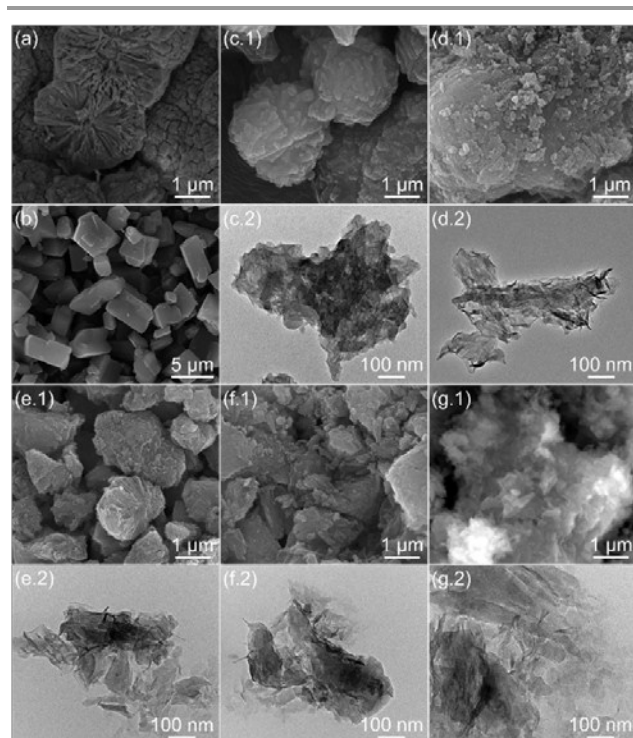

Fig. 2. SEM images of (a) MIL-68(Al)as, (b) MIL-53(Al)as, (c.1) US-60°C-45min, (d.1) ST-RT-3d, (e.1) ST-RT-12d, (f.1) ST-RT-30d and (g.1) REF-60°C-14d. TEM images of (c.2) US-60°C-45min, (d.2) ST-RT-3d, (e.2) ST-RT-12d, (f.2) ST-RT-30d and (g.2) REF-60°C-14d.
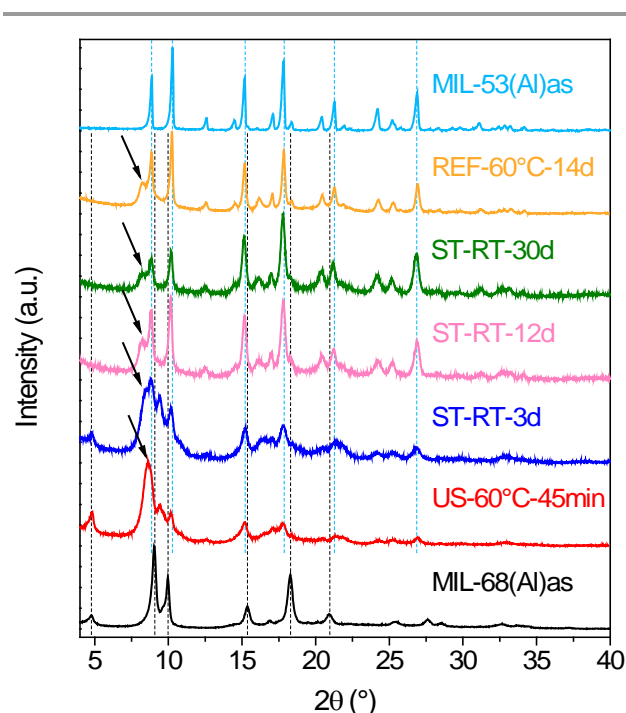

Fig. 3. PXRD patterns of MIL-68(Al)as, MIL-53(Al)as and the intermediate products. The unknown phase is marked with black arrows.

ARTICLE

corresponded to the unknown phase, which was maintained with time. However, after a short period of time (a few seconds) of beam exposition (*t* = t), some of the spots appeared diffused (Fig. 4g). Additionally, the d-spacing corresponding to plane (101) of MIL-53(Al)as suffered a contraction, which also affected plane (202). This observation suggests that the nanosheets evolve with the electron beam producing the structure deformation. By applying Fast Fourier Transform (FFT) analysis, the diffraction pattern was shown to be very diffuse suggesting d-spacings higher than expected. This was attributed to a possible overlapping of nanosheets, which also implies an overlapping of crystallographic planes. Volkringer *et al*. studied the thermal behaviour of Ga- and In-based MIL-68 MOFs by thermodiffractometry.[54] MIL-68(Ga) was stable up to 350 °C without changes in the peaks. However, a second contribution with a broad reflection was observed from 200 °C at 2θ ≈ 8.0° which moved to lower angles (2θ ≈ 7.8°) at higher temperatures. The presence of this unidentified peak was ascribed to a slow phase transition towards the MIL-68(Ga) collapse. MIL-68(In) did not suffer such behaviour. In our case, the unknown reflection might also be related to a transition phase towards the structure collapse caused by the different treatments in water. Since its intensity was reduced as the conditions became more severe, it is thought that the collapse was slowed down as the MIL-53(Al)as structure was being acquired. It is worth mentioning that the intermediate products were not as crystalline as MIL-53(Al)as because of the relatively low crystallinity (broad PXRD peaks, see Fig. 3) of the starting MIL-68(Al)as material. In any event, these TEM and electron diffraction features confirming that the nanosheets possess the structure of the 3D MIL-53(Al) allow to infer that the pore size of the new material should coincide with that of MIL-53(Al), i.e. ca. 0.85 nm.[5, 24]

The ^{13}C NMR (CP-MAS and [1]H-decoupled) spectra of MIL-68(Al)as and an intermediate product, ST-RT-12d, are displayed in Fig. 5. The MIL-68(Al)as spectrum showed a signal at a chemical shift of 170 ppm assigned to the carbon of the carboxylate (-COO) function.[24] The signals between 141 and 122 ppm were due to the aromatic (-CH) and quaternary carbons.[24] The signal placed at 162 ppm was caused by the carbon of the amide group (-CON-) of the DMF molecules retained in the MIL-68(Al)as pores. The ST-RT-12d had a slightly different ^{13}C NMR spectrum than that of the as-made MIL-68(Al) (see Fig. 5). ST-RT-12d also had signals at 170 ppm and 141-122 ppm deriving from the carbons of the carboxylate group and the aromatic ring, respectively. However, the signal at 129 ppm in the CP-MAS spectrum (aromatic carbons, -CH) was split (black arrow) owing to the presence of carboxylates in both protonated and deprotonated forms from guest terephthalic acid molecules and ligand terephthalate anions, respectively.[24] This confirms that terephthalic acid was formed and trapped in the pores of ST-RT-12d. A new signal arose at a chemical shift of 174 ppm corresponding to the carbon of the carboxylate function interacting with water molecules adsorbed in the pores.[24] The characteristic signal of DMF disappeared, as expected. The ^{13}C NMR results corroborated the MIL-68(Al) conversion towards MIL-53(Al), the terephthalic acid formation and the presence of water in the pores, in agreement with the FTIR, TGA and PXRD characterization. Unlike MIL-53(Al)as, the intermediate products contained terephthalic acid as well as water molecules in their pores.

MIL-68(Al)as and MIL-53(Al)np displayed type I isotherms, common in microporous materials (Fig. S5). The BET and external areas are summarized in table S1. The obtained BET areas were lower than other reported values.[24, 49] This is probably due to a non-complete removal of guest molecules from the MOF pores. The intermediate products featured a combination of type I and type IV isotherms, the latter being characteristic of the presence of mesoporosity (Fig. S5). MIL-53(Al)np and MIL-68(Al)as did not present any hysteresis. However, the intermediate products had hystereses which were closed near saturation, belonging to type H-3. The
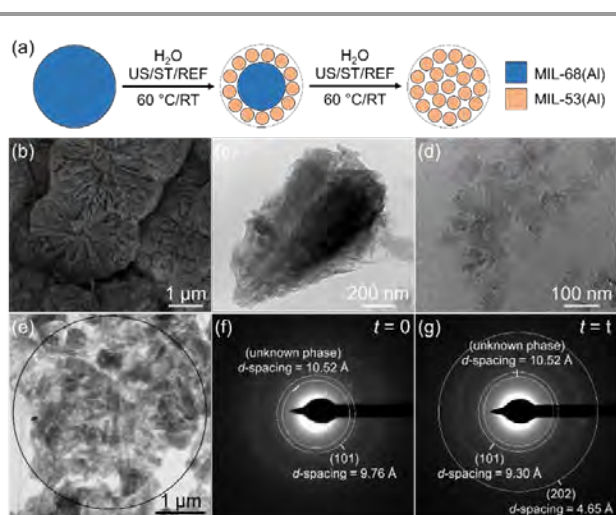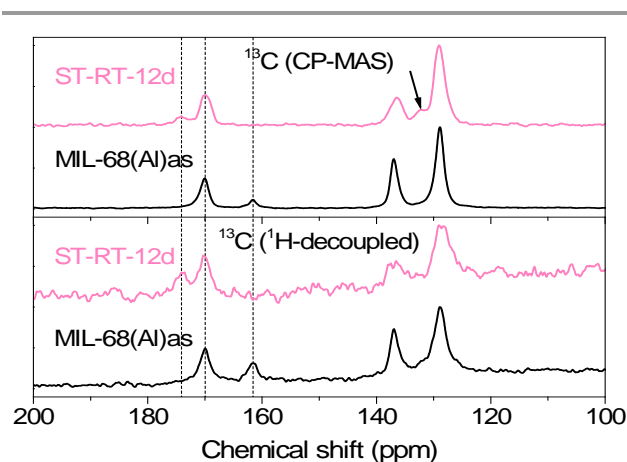

Fig. 4. (a) Schematic shrinking core model for the transformation from MIL-68(Al) to MIL-53(Al). (b) SEM image of MIL-68(Al)as. (c) TEM image of ST-RT-30d. (d) TEM image of REF-60°C-14d. Images (b), (c) and (d) correspond to the first, second and third states, respectively, in the shrinking core model scheme of (a). (e) Selected area in electron diffraction analysis. Electron diffraction patterns at (f) *t* = 0 and (g) *t* = t.

Fig. 5. 13C NMR (CP-MAS and 1H-decoupled) spectra of MIL-68(Al)as and ST-RT-12d.

ARTICLE

hysteresis loops were more pronounced at high values of relative pressures (p/p₀ > 0.8) and when the treatment conditions became more severe. As MIL-68(Al) and MIL-53(Al) are microporous, the mesoporosity of the intermediate products is ascribed to intercrystalline or interlamellar voids. This is consistent with the SEM and TEM images which confirm the formation of thin 2D particles. It is possible to relate the external area and the particle size of solids; the smaller the particle size, the higher the external area. Fig. 6 compares the external (S_{ext}) and BET (S_{BET}) specific surface areas of MIL-68(Al)as, MIL-53(Al)np and the intermediate products. The results are in good agreement with the SEM and TEM observations. The MIL-53(Al)as crystals were larger than those of MIL-68(Al)as. Consequently, the external area of MIL-53(Al)np was lower than that of MIL-68(Al)as. When MIL-68(Al)as was immersed into water under stirring at room temperature (ST-RT-3/12/30d), the external area increased over time because the crystal size was reduced and a larger amount of nanosheets (see above TEM observations) was produced. Lower external areas were achieved with ST-RT-30d and REF-60°C-14d (more severe conditions) than with ST-RT-12d. Regarding the BET surface areas (Fig. 6 and table S1), all the intermediate products exhibited lower values than those of MIL-68(Al)as and MIL-53(Al)np. The maximum BET surface was achieved with ST-RT-30d (875 m² g⁻¹), although this value was far away from that of MIL-53(Al)np (1051 m² g⁻¹), so that the period of 30 d was not enough for a complete conversion from MIL-68(Al) to MIL-53(Al). As can be seen, the treatment at 60 °C for 14 d (REF-60°C-14d) produced slightly lower BET and external surface areas than those of ST-RT-30d (828 *vs*. 875 m² g⁻¹ and 141 *vs*. 151 m² g⁻¹, respectively).

Insight into the transformation from MIL-68(Al) to MIL-53(Al)

According to the TEM, SEM and N_2 sorption results, the transformation from MIL-68(Al) to MIL-53(Al) is thought to have taken place as follows. The external layer of the crystals underwent the transformation first, being converted partially into MIL-53(Al). The outer crystals (intermediate products) were delaminated, producing nanosheets of MIL-53(Al) (observed in the TEM images of Fig. 2) and leaving a non-reacted core. The transformation from MIL-68(Al) to MIL-53(Al) is assumed to follow a shrinking core model (Fig. 4a). According to this model, the reaction occurs first at the outer layer of the particle. The reaction zone moves into the particle, so that the solid core shrinks progressively while growing a surrounding coating of converted and inert product.[55] It must be taken into consideration that the MIL-53(Al) structure (0.85 nm pores)[5, 24] is denser than that of MIL-68(Al) (0.6-0.64 and 1.6-1.7 nm pores).[21] This would have provoked an increase in the mass transport resistance parallel to the advance of the reaction, justifying that the transformation was never completed, even after one month of exposure, as seen above.

Regarding the reaction, the crystalline conversion from MIL-68(Al) to MIL-53(Al) is thought to have taken place through a reorganization of the octahedra inorganic chains after dissolution of DMF molecules by water molecules (Fig. 7). Since DMF molecules serve as a template for the triangular pores,[20]
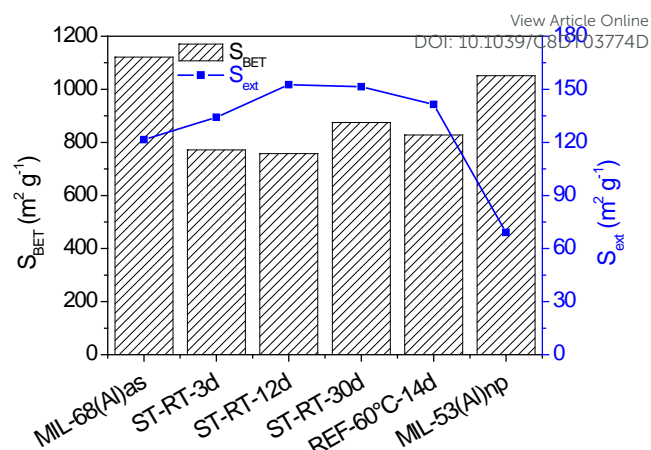
Fig. 6. BET (S_{BET}) and external (S_{ext}) specific surface areas of MIL-68(Al)as, MIL-53(Al)np and the intermediate products.

when they were dissolved by water, the MIL-68(Al)as structure became unstable. Some ligand-inorganic chain bonds broke and the free inorganic chains were rearranged in the middle of the hexagonal channels and recoordinated by surrounding terephthalate ions (Fig. 7a). Then, there was a global contraction movement in the network where some linked chains were moved to the hexagonal pore centres sweeping along the crystalline structure, that is, other ligand-inorganic chain bonds (Fig. 7b). Finally, the ligand-inorganic chain linkages separating the triangular pores broke and the one-end free ligands were bound to the available inorganic chains, delimiting rhombic channels (Fig. 7c). Some terephthalate ligands (maybe terminal ligands) were lost during the transformation and were hydrolysed by water giving rise to terephthalic acid molecules inside the pores. As seen by the FTIR, TGA and NMR characterization, some terephthalic acid was encapsulated along with the water molecules. Inorganic octahedra could also have suffered hydrolysis leading to water-soluble ionic complexes which had been removed upon centrifugation.
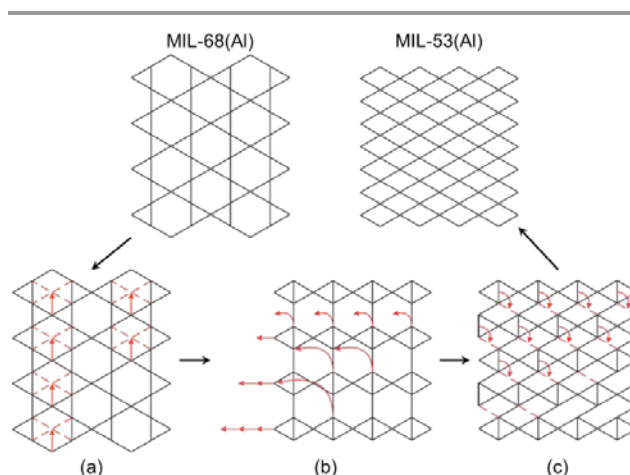
Fig. 7. Scheme of the mechanism proposed for the transformation from MIL-68(Al) to MIL-53(Al). Terephthalic acid, DMF and water guest molecules are omitted for clarity.

Membrane characterization

The activated and disaggregated materials ST-RT-30d-ns and REF-60°C-14d-ns were employed to fabricate PDMS-MMMs (ST-RT-30d-ns_m and REF-60°C-14d-ns_m, respectively) on polyimide supports in order to study their performance in the separation of CO_2/N_2 and CO_2/CH_4 binary mixtures. A bare membrane with PDMS only and a membrane with MIL-53(Al)np (MIL-53(Al)np_m) were similarly prepared for comparison. Several techniques were used to carry out the characterization of the membranes. The ATR-FTIR and TGA results are discussed in detail in the captions of Figs. S6 and S7, respectively.

PXRD patterns of the membranes are shown in Fig. 8. The bare membrane showed a broad amorphous band with a weak peak at 2θ = 5.5°. This peak was also observed in the MIL-53(Al)np_m. The pattern of REF-60°C-14d-ns_m preserves the peak marked with an arrow (8.2°) corresponding to the unknown phase (d-spacing ~10.5 Å), as previously explained in the discussion of the electron diffraction characterization (Fig. 4). In the case of ST-RT-30d-ns_m, this signal and the peak from the bare membrane (5.5°) could be overlapped by the background noise. MIL-53(Al)np_m had two strong peaks (8.7 and 17.3°) while the others were all weak. This difference in the relative intensity of the peaks was caused by a preferential orientation of the MIL-53(Al)np crystals. These crystals were oriented with the b axis, and thus the pore channels, parallel to the polyimide surface and/or forming an angle of 45° (see Fig. 8). The presence of several peaks from both simulated MIL-

53(Al)lp and MIL-53(Al)as was evident for MIL-53(Al)np_m and REF-60°C-14d-ns_m. These peaks were also noticeable for ST-RT-30d-ns_m but weaker and broader. This could be due to a more limited coverage of the support surface with nanosheets. It is worth mentioning that the appearance of well-differentiated peaks implies that the crystallinity of the selective materials was preserved. The patterns of the membranes with MIL-53(Al)np and the disaggregated nanosheets of the intermediate products thus appear to be a combination of those of MIL-53(Al)as and MIL-53(Al)lp, also confirmed by electron diffraction. However, some reflections in the patterns of the membranes were displaced in comparison with those of the reference materials (MIL-53(Al)as and MIL-53(Al)lp). MIL-53(Al)np, ST-RT-30d-ns and REF-60°C-14d-ns had contracted pores filled with water molecules before the membrane fabrication. As stated above, it is thought that PDMS polymeric chains (with a 0.7-0.8 nm diameter[56] not too far from the MIL-53(Al) pore dimensions of 0.85 nm) filled and opened the outer pores of the particles in the membranes, while the inner pores remained in the np form, resulting in an intermediate structure between MIL-53(Al)np and MIL-53(Al)lp. This was supported by the ATR-FTIR results (Fig. S6), which have suggested a structure similar to that of MIL-53(Al)as for the fillers, and is in agreement with Hsieh et al. who combined MIL-53(Al) in the as, np and lp phases with Matrimid® for gas separation.[57]

The top view and cross-sectional SEM images of MIL-53(Al)np_m, ST-RT-30d-ns_m and REF-60°C-14d-ns_m are shown in Fig. 9. The MIL-53(Al)np crystals covered the support surface completely (Fig. 9a.1). PDMS was noticed as the crystal edges were not well-distinguished. Most of the crystals were similarly arranged in the MMM, corroborating the preferential orientation seen by PXRD (Fig. S4 and Fig. 8). Regarding the intermediate products, both ST-RT-30d-ns_m and REF-60°C-14d-ns_m had particles distributed over the support surface, although some agglomerates protruded out from the surface (Fig. 9b.1 and c.1). The SEM images did not show single nanosheets of the intermediate products. It seems that delaminated crystals formed agglomerates of different sizes. The lower crystal loading in ST-RT-30d-ns_m (Fig. 9b.1) and/or a higher amount of PDMS (Fig. 9b.2) could have caused the weak intensity of the peaks and bands in the corresponding PXRD pattern (Fig. 8) and ATR-FTIR spectrum (Fig. S6), respectively. The PDMS was noticed in both cases as a film covering the surface. The thickness of the PDMS-crystal layer of the three membranes was measured from the cross-sectional SEM images (second row from top in Fig. 9), giving 10.1 ± 1.9 μm, 6.8 ± 1.7 μm and 5.4 ± 1.9 μm for MIL-53(Al)np_m, ST-RT-30d-ns_m and REF-60°C-14d-ns_m, respectively. The larger thickness in MIL-53(Al)np_m was ascribed to the larger crystal size. The PDMS layer of the bare membrane had a non-uniform thickness reaching values of ca. 4.5 μm (Fig. S8). The cross-section images indicated a good adherence of PDMS to the polyimide support for MIL-53(Al)np_m and REF-60°C-14d-ns_m. These images also showed the asymmetric nature of the polyimide supports with a denser layer on top and a porous structure with fingers at the bottom. The EDX composition lines
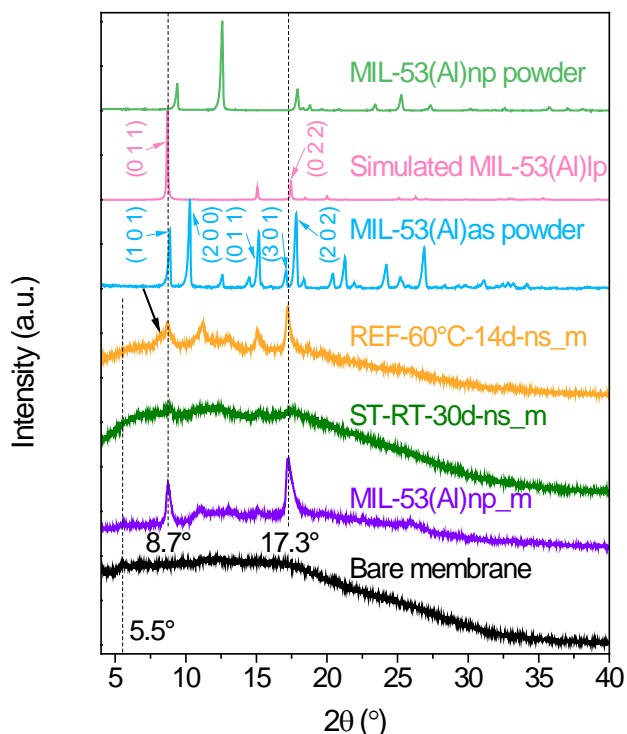

Fig. 8. PXRD patterns of MIL-53(Al)np powder, simulated MIL-53(Al)lp (CCDC 220476),[24] the bare membrane and the membranes prepared with MIL-53(Al)np (MIL-53(Al)np_m), ST-RT-30d-ns (ST-RT-30d-ns_m) and REF-60°C-14d-ns (REF-60°C-14d-ns_m).
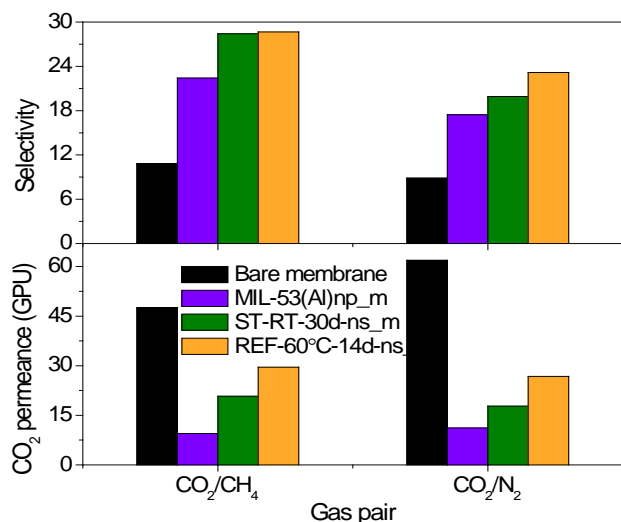
Journal Name

ARTICLE

Fig. 10. CO_2 permeance and selectivity results for the different membranes in the gas separation of CO_2/CH_4 and CO_2/N_2.

Fig. 9. (1) Top view, (2) cross-sectional and (3) composition line SEM images of: (a) MIL-53(Al)np_m, (b) ST-RT-30d-ns_m and (c) REF-60°C-14d-ns_m. The thicknesses appearing in the cross-sectional SEM images (second row from top) correspond to the MMMs (filler + PDMS).

in Fig. 9 (last row) show a higher concentration of Al in the areas corresponding to the supported MMMs coming from the MOF fillers. It is also seen that PDMS penetrated into the polyimide support in the four membranes, probably sealing the polyimide defects, as Zulhairun *et al*. made with asymmetric polysulfone containing HKUST-1 crystals.[58]

The process followed in the fabrication of the membranes with MIL-53(Al)np and both intermediate products led to a supported-MMM. This method enabled lower thicknesses to be achieved than those of the MMMs prepared conventionally, in addition to good MOF coatings. The polyimide supports improve the mechanical resistance of the thin, flexible MMMs. The flexibility is provided by the PDMS polymer.

Gas mixture separation

The membranes prepared with both ST-RT-30d-ns and REF-60°C-14d-ns were used in the separation of CO_2/CH_4 and CO_2/N_2 in order to study their performance. The corresponding results were compared to those obtained with the bare and MIL-53(Al)np membranes (Fig. 10 and table S3). Gas mixture tests have been preferred since they describe a more realistic behaviour that ideal selectivities. However, a dense PDMS membrane has been tested to obtain both ideal and real selectivities. The results are shown in table S2, where it can be seen how there almost no differences. The permeance and selectivity values of the polyimide support are not shown because it was not selective to any gas component (selectivity ≈

1). The bare membrane (PDMS + polyimide P84®) showed selectivities of 10.8 and 8.9 for the CO_2/CH_4 and CO_2/N_2 mixtures, respectively. This means that PDMS penetrated deeply into the polyimide support, as seen by EDX, sealing the defects. PDMS, a rubbery polymer having flexible chains,[59] favoured suitable wetting with good MOF-PDMS and PDMS-polyimide adherences, rendering homogeneous membranes with good dispersion of particles.[60] The CO_2/CH_4 and CO_2/N_2 selectivities increased by at least two-fold for the MOF-loaded membranes (22.4-28.7 *vs*. 10.8 and 17.5-23.2 *vs*. 8.9, respectively) compared to the bare membrane. In addition, the MMM with MIL-53(Al) nanosheets improved the CO_2/CH_4 (28.4-28.7 vs. 22.4) and CO_2/N_2 (19.9-23.2 vs. 17.5) selectivities of the conventional MIL-53(Al) MMM with higher CO_2 permeances (20.8-29.6 GPU vs. 9.5 GPU for CO_2/CH_4 and 17.7-26.8 GPU vs. 11.2 GPU for CO_2/N_2).

The selectivities and permeances of the MMMs increased and decreased, respectively, for all gases and mixtures in comparison with those of the bare membrane (Fig. 10 and table S3). Rigidification[61] and pore blocking[62] are profiled as the possible causes. However, the permeances of CO_2, CH_4 and N_2 through the three MOF-loaded membranes decreased by 38-82, 77-90 and 83-91 %, respectively (table S4). These percentages are significantly high (but lower for CO_2, probably due to the important CO_2 adsorption properties of MIL-53(Al).[63]), suggesting pore blocking. The kinetic diameters of the studied gases (CO_2, 3.3 Å; N_2, 3.6 Å; CH_4, 3.8 Å),[24] are much lower than the pore size of MIL-53(Al) (ca. 8.5 Å),[24] so that PDMS polymeric chains were assumed to have penetrated into the pores, largely narrowing the pore size. This provoked a gas separation based on size exclusion. PDMS produced a good wetting around the particles and its flexible chains were capable of reaching the pore inside. This is in accordance with the ATR-FTIR and PXRD characterization of the membranes. It is thought that PDMS filled, opened and simultaneously narrowed the outer pores of MIL-53(Al)np, ST-RT-30d-ns and REF-60°C-14d-ns when preparing the membranes, while the other inner pores retained the np form. Consequently, an intermediate structure between the np and the as or lp phases was assumed to have been formed.

The permeation results of MIL-53(Al)np_m, ST-RT-30d-ns_m and REF-60°C-14d-ns_m (Fig. 10 and table S3) showed that both intermediate products improved the performance of MIL-53(Al)np_m, achieving the best values with REF-60°C-14d-ns_m. It is thought that the crystal orientation in the membranes was the crucial key. As mentioned above, micron size crystals in MIL-53(Al)np_m were preferentially oriented with the b axis and the unidimensional pores parallel to the support surface and/or forming 45° (Fig. 1a, Fig. S4 and Fig. 8). This hindered the gas diffusion through the membrane and increased the pathlength of the gas molecules. The higher permeances of ST-RT-30d-ns_m and REF-60°C-14d-ns_m are consistent with the preferential arrangement of MIL-53(Al) nanosheets parallel to the polyimide support, with their channels aligned with the flow direction, favouring rapid gas diffusion. The smaller thicknesses of ST-RT-30d-ns_m and REF-60°C-14d-ns_m (6.8 ± 1.7 µm and 5.4 ± 1.9 µm, respectively) compared to that of MIL-53(Al)np_m

ARTICLE

(10.1 ± 1.9 µm) may also have contributed to the increase in permeance.

REF-60°C-14d-ns_m was superior to ST-RT-30d-ns_m in both permeance and selectivity. This is in line with the fact that the diffraction peaks and ATR-FTIR bands of REF-60°C-14d-ns_m were more intense. In addition, it is supposed that a better distribution of the particles over the support surface and an improved PDMS-polyimide adherence, as seen by SEM, caused the enhancement in the gas separations. The better distribution was due to lower nanosheet agglomeration[64] in the PDMS-filler dispersion when preparing REF-60°C-14d-ns_m (as seen in Fig. S1, the nanosheet suspension of REF-60°C-14d-ns in ethanol was more stable than that of ST-RT-30d-ns with a lower amount of precipitates after 21 d).

A comparison of the permeation results of several MMMs containing MIL-53(Al) as the filler or PDMS as the polymeric matrix in CO_2/CH_4 and CO_2/N_2 separations is shown in table S5 and table S6, respectively. Regarding the CO_2/CH_4 separation (table S5), the ideal selectivities of the binary gas experiments obtained with the intermediate products improved those of the MIL-53(Al) MMMs prepared with 6FDA/ODA-DAM,[65] reaching the same values as those achieved with Matrimid®-based MMMs.[65] The hybrid composite membranes also improved the ideal selectivities of the MMMs prepared using the amino-functionalized MIL-53(Al) and Ultem®[65] or 6FDA/ODA-DAM.[65] The CO_2 permeability of ST-RT-30d-ns_m and REF-60°C-14d-ns_m was determined using the MMM thickness (MOF + PDMS) estimated from SEM images in order to establish a comparison. As seen, the CO_2 permeability of ST-RT-30d-ns_m and REF-60°C-14d-ns_m was higher than that reported for the different MOFs and polymers.[65-68] With regard to the CO_2/N_2 gas mixture (table S6), the MMMs with the MIL-53(Al) nanosheets had higher ideal selectivities than the selectivity achieved with the HKUST-1-PDMS MMMs in single gas tests.[68] The CO_2 permeances through ST-RT-30d-ns_m and REF-60°C-14d-ns_m were higher than those through the MIL-53(Al)-Matrimid® membranes[66] and were within the range of the MIL-53(Al)-Ultem® MMMs.[69]

The success of the hybrid composite membranes was due to a combination of different factors: the MOF MIL-53(Al) in question, that enhanced the CO_2 solubility of the resulting membranes by its important CO_2 adsorption properties,[63] the crystal morphology and orientation, the microporosity of the filler, the PDMS-polyimide synergy and the continuous MOF coatings wrapped by PDMS. The method used in this work to prepare hybrid composite membranes could be applied to other MOFs.

Conclusions

Several characterization techniques (FTIR, ATR-FTIR, TGA, SEM, TEM, PXRD, NMR, adsorption) have indicated that the transformation from MIL-68(Al) to MIL-53(Al) by direct soaking in water was not complete and followed a crackling core model. The transformation was studied under different conditions (stirring, reflux, ultrasound, room temperature, 60 °C) and the more severe conditions led to the more converted products. Needle-shaped MIL-68(Al) crystals forming spherical aggregates

were delaminated during the transformation, giving rise to MIL-53(Al) nanosheets. These were used to prepare PDMS-based MMMs supported on polyimide P84® by vacuum filtration. For comparison, a membrane with activated MIL-53(Al) was similarly fabricated. The membranes were characterized to examine the PDMS-polyimide and PDMS-particle adherence. Vacuum filtration caused PDMS to penetrate into the polyimide support, sealing the defects. The composite membranes were applied to the separation of CO_2/N_2 and CO_2/CH_4 mixtures, showing higher selectivity than that afforded by the bare membrane and the activated MIL-53(Al) membrane. The permeance values were lower than that of the bare membrane but higher than that of the activated MIL-53(Al) MMM. PDMS polymeric chains penetrated into the outer pores of the filler crystals causing their partial blocking and increasing the pore size in such a way that an intermediate structure between the np and the as or lp phases of MIL-53(Al) was accomplished. Crystals in the activated MIL-53(Al) membrane were preferentially oriented with the unidimensional pores arranged parallel and/or at 45° with the support surface, hindering the gas flow. The higher permeances of MMMs prepared with MIL-53(Al) nanosheets (as compared to those MMMs with MIL-53(Al) microsized crystals) are consistent with the preferential arrangement of such nanosheets parallel to the polyimide support, with their channels aligned with the flow direction, enabling selective gas transport. The improved performance of the composite membranes prepared with the disaggregated nanosheets of the intermediate products was a result of the crystal morphology and orientation, the pore blocking phenomenon, the PDMS-sealed polyimide support and the uniformly covered support with the MOF wrapped by PDMS. Finally, in the field of mixed matrix membranes, 2D materials open the possibility of producing ultrathin membranes with minimum amount filler and better separation performance.

Acknowledgements

Notes and references

1   P. Amo-Ochoa and F. Zamora, *Coord. Chem. Rev.,* 2014, **276**, 34-58.

2   M. Shah, M. C. McCarthy, S. Sachdeva, A. K. Lee, and H. K. Jeong, *Ind. Eng. Chem. Res.*, 2012, **51**, 2179-2199.

3   G. Yilmaz, A. Ozcan and S. Keskin, *Mol. Simul.,* 2015, **41**, 713-726.

4   J. Cravillon, R. Nayuk, S. Springer, A. Feldhoff, K. Huber and M. Wiebcke, *Chem. Mater.,* 2011, **23**, 2130-2141.

5   C. Serre, F. Millange, C. Thouvenot, M. Nogues, G. Marsolier, D. Louer and G. Ferey, *J. Am. Chem. Soc.,* 2002, **124**, 13519-13526.

6   S. Kitagawa, R. Kitaura and S. Noro, *Angew. Chem., Int. Ed.,* 2004, **43**, 2334-2375.

7   S. L. Qiu and G. S., *Coord. Chem. Rev.,* 2009, **253**, 2891-2911.

8   D. Y. Hong, Y. K. Hwang, C. Serre, G. Ferey and J. S. Chang, *Adv. Funct. Mater.,* 2009, **19**, 1537-1552.

9   W. Xuan, C. Zhu, Y. Liu and Y. Cui, *Chem. Soc. Rev.,* 2012, **41**, 1677-1695.

10   H. J. Park, D.-W. Lim, W. S. Yang, T-R. Oh, and M. P. A. Suh, *Chem. - Eur. J.,* 2011, **17**, 7251-7260.

11   L. M. Huang, H. T. Wang, J. X. Chen, Z. B. Wang, J. Y. Sun, D. Y. Zhao and Y. S. Yan, *Microporous Mesoporous Mater.,* 2003, **58**, 105-114.

12   J. R. Li, R. J. Kuppler and H. C. Zhou, *Chem. Soc. Rev.,* 2009, **38**, 1477-1504.

13   N. Liedana, A. Galve, C. Rubio, C. Tellez and J. Coronas, *ACS Appl. Mater. Interfaces,* 2012, **4**, 5016-5021.

14   L. Paseta, E. Simon-Gaudo, F. Gracia-Gorria and J. Coronas, *Chem. Eng. J.,* 2016, **292**, 28-34.

15   S. Biswas, S. Couck, M. Grzywa, J. F. M. Denayer, D. Volkmer and P. Van der Voort, *Eur. J. Inorg. Chem.,* 2012, 2481-2486.

16   B. Moulton and M. J. Zaworotko, *Chem. Rev.,* 2001, **101**, 1629-1658.

17   S. A. Barnett, A. J. Blake, N. R. Champness and C. Wilson, *Chem. Commun.,* 2002, 1640-1641.

18   A. J. Blake, N. R. Brooks, N. R. Champness, M. Crew, A. Deveson, D. Fenske, D. H. Gregory, L. R. Hanton, P. Hubberstey and M. Schroder, *Chem. Commun.,* 2001, 1432-1433.

19   T. A. Makal, A. A. Yakovenko and H. C. Zhou, *J. Phys. Chem. Lett.* 2011, **2**, 1682-1689.

20   A. Fateeva, P. Horcajada, T. Devic, C. Serre, J. Marrot, J.-M. Greneche, M. Morcrette, J.-M. Tarascon, G. Maurin and G. Ferey, *Eur. J. Inorg. Chem.,* 2010, 3789-3794.

21   K. Barthelet, J. Marrot, G. Ferey and D. Riou, *Chem. Commun.,* 2004, 520-521.

22   Y. Hu, B. Lin, P. He, Y. Y. Li, Y. N. Huang and Y. Song, *Chem. - Eur. J.,* 2015, **21**, 18739-18748.

23   P. L. Llewellyn, P. Horcajada, G. Maurin, T. Devic, N. Rosenbach, S. Bourrelly, C. Serre, D. Vincent, S. Loera-Serna, Y. Filinchuk and G. Ferey, *J. Am. Chem. Soc.,* 2009, **131**, 13002-13008.

24   T. Loiseau, C. Serre, C. Huguenard, G. Fink, F. Taulelle, M. Henry, T. Bataille and G. Ferey, *Chem. - Eur. J.,* 2004, **10**, 1373-1382.

25   A. E. Khudozhitkov, H. Jobic, D. Freude, J. Haase, D. I. Kolokolov and A. Stepanov, *J. Phys. Chem. C,* 2016, **120**, 21704-21709.

26   X. Huang, P. Sheng, Z. Tu, F. Zhang, J. Wang, H. Geng, Y. Zou, C.-A. Di, Y. Yi, Y. Sun, W. Xu and D. Zhu, *Nat. Commun.,* 2015, **6**, 1-8.

27   B. C. R. Camacho, R. Ribeiro, I. Esteves and J. P. B. Mota, *Sep. Purif. Technol.,* 2015, **141**, 150-159.

28   B. Seoane, V. Sebastian, C. Tellez and J. Coronas, *CrystEngComm,* 2013, **15**, 9483-9490.

29   L. F. Zhu, H. W. Yu, H. J. Zhang, J. N. Shen, L. X. Xue, C. J. Gao and B. van der Bruggen, *RSC Adv.,* 2015, **5**, 73068-73076.

30   C. Echaide-Gorriz, S. Sorribas, C. Tellez and J. Coronas, *RSC Adv.,* 2016, **6**, 90417-90426.

31   L. Xie, D. Liu, H. Huang, Q. Yang and C. Zhong, *Chem. Eng. J.,* 2014, **246**, 142-149.

32   M. S. Tehrani and R. Zare-Dorabei, *Spectrochim. Acta, Part A,* 2016, **160**, 8-18.

33   L. Mitchell, B. Gonzalez-Santiago, J. P. S. Mowat, M. E. Gunn, P. Williamson, N. Acerbi, M. L. Clarke and P. A. Wright, *Catal. Sci. Technol.,* 2013, **3**, 606-617.

34   J.-R. Li, J. Sculley and H.-C. Zhou, *Chem. Rev.,* 2012, **112**, 869-932.

35   B. Zornoza, C. Tellez, J. Coronas, J. Gascon, F. Kapteijn, *Microporous Mesoporous Mater.,* 2013, **166**, 67-78.

36   Z. Yin and M. Zeng, *Sci. China: Chem.,* 2011, **54**, 1371-1394.

37   J. P. Zhang, P. Q. Liao, H. L. Zhou, R. B. Lin and X. M. Chen, *Chem. Soc. Rev.,* 2014, **43**, 5789-5814.

38   M.-H. Zeng, S. Hu, Q. Chen, G. Xie, Q. Shuai, S.-L. Gao and L.-Y. Tang, *Inorg. Chem.,* 2009, **48**, 7070-7079.

39   M. K. Sharma, P. Lama and P. K. Bharadwaj, *Cryst. Growth Des.,* 2011, **11**, 1411-1416.

40   F. Carson, J. Su, A. E. Platero-Prats, W. Wan, Y. Yun, L. Samain and X. Zou, *Cryst. Growth Des.,* 2013, **13**, 5036-5044.

41   E. Stavitski, M. Goesten, J. Juan-Alcaniz, A. Martinez-Joaristi, P. Serra-Crespo, A. V. Petukhov, J. Gascon and F. Kapteijn, *Angew. Chem., Int. Ed.,* 2011, **50**, 9624-9628.

42   S. Choi, H. J. Lee, T. Kim and M. Oh, *Eur. J. Inorg. Chem.,* 2014, 6220-6224.

43   N. Liedana, P. Lozano, A. Galve, C. Tellez and J. Coronas, *J. Mater. Chem. B,* 2014, **2**, 1144-1151.

44   A. Perea-Cachero, E. Romero, C. Tellez and J. Coronas, *CrystEngComm,* 2018, **20**, 402-406.

45   M. Kriesten, K. Hoffmann and M. Hartmann, *CrystEngComm,* 2018, **20**, 3117-3119.

46   K. V. Agrawal, X. Zhang, B. Elyassi, D. D. Brewer, M. Gettel, S. Kumar, J. A. Lee, S. Maheshwari, A. Mittal, C.-Y. Sung, M. Cococcioni, L. F. Francis, A. V. McCormick, K. A. Mkhoyan and M. Tsapatsis, *Science,* 2011, **334**, 72-75.

47   J. J. Low, A. I. Benin, P. Jakubczak, J. F. Abrahamian, S. A. Faheem and R. R. Willis, *J. Am. Chem. Soc.,* 2009, **131**, 15834-15842.

48   T. Rodenas, I. Luz, G. Prieto, B. Seoane, H. Miro, A. Corma, F. Kapteijn, F. X. Llabres i Xamena, J. Gascon, *Nat. Mater.,* 2015, **14**, 48-55.

49   Q. Yang, S. Vaesen, M. Vishnuvarthan, F. Ragon, C. Serre, A. Vimont, M. Daturi, G. De Weireld and G. Maurin, *J. Mater. Chem.,* 2012, **22**, 10210-10220.

50   H. Putz and K. Brandenburg, *Diamond - Crystal and Molecular Structure Visualization, Version 4.2.2,* Crystal Impact, Bonn, Germany, 2016.

51   C. A. Schneider, W. S. Rasband and K. W. Eliceiri, *Nat. Methods,* 2012, **9**, 671-675.

52   W. D. Harkins and G. Jura, *J. Am. Chem. Soc.,* 1944, **66**, 1366-1373.

53   F. Zhang, X. Zou, F. Sun, H. Ren, Y. Jiang and G. Zhu, *CrystEngComm,* 2012, **14**, 5487-5492.

54   C. Volkringer, M. Meddouri, T. Loiseau, N. Guillou, J. Marrot, G. Ferey, M. Haouas, F. Taulelle, N. Audebrand and M. Latroche, *Inorg. Chem.,* 2008, **47**, 11892-11901.

55   J. Y. Park and O. Levenspiel, *Chem. Eng. Sci.,* 1975, **30**, 1207-1214.

56   B. Erman and J. E. Mark, Swelling of Networks. *Structures and Properties of Rubberlike Networks,* 1st ed; Oxford University Press, Inc.: New York, 1997.

Dalton Transactions Accepted Manuscript

57   J. O. Hsieh, K. J. Balkus, J. P. Ferraris and I. H. Musselman, *Microporous Mesoporous Mater.,* 2014, **196**, 165-174.
58   A. K. Zulhairun, Z. G. Fachrurrazi, M. N. Izwanne and A. F. Ismail, *Sep. Purif. Technol.,* 2015, **146**, 85-93.
59   J. H. Wang, Y. Li, Z. S. Zhang and Z. P. Hao, *J. Mater. Chem. A,* 2015, **3**, 8650-8658.
60   H. W. Fan, N. X. Wang, S. L. Ji, SL, H. Yan and G. J. Zhang, *J. Mater. Chem. A.,* 2014, **2**, 20497-20957.
61   T. T. Moore and W. J. Koros, *J. Mol. Struct.,* 2005, **739**, 87-98.
62   T.-S. Chung, L. Y. Jiang, Y. Li and S. Kulprathipanja, *Prog. Polym. Sci.,* 2007, **32**, 483-507.
63   J. Liu, P. K. Thallapally, B. P. McGrail, D. R. Brown and J. Liu, *Chem. Soc. Rev.,* 2012, **41**, 2308-2322.
64   J. Sanchez-Lainez, B. Zornoza, A. Mayoral, A. Berenguer-Murcia, D. Cazorla-Amoros, C. Tellez and J. Coronas, *J. Mater. Chem. A,* 2015, **3**, 6549-6556.
65   X. Y. Chen, V. T. Hoang, D. Rodrigue and S. Kaliaguine, *RSC Adv.,* 2013, **3**, 24266-24279.
66   H. Q. Ren, J. Y. Jin, J. Hu and H. L. Liu, *Ind. Eng. Chem. Res.,* 2012, **51**, 10156-10164.
67   E. A. Feijani, A. Tavasoli and H. Mahdavi, *Ind. Eng. Chem. Res.,* 2015, **54**, 12124-12134.
68   B. Li, H. L. Wang and B. L. Chen, *Chem. - Asian J.,* 2014, **9**, 1474-1498.
69   H. T. Zhu, L. N. Wang, X. M. Jie, D. D. Liu and Y. M. Cao, *ACS Appl. Mater. Interfaces,* 2016, **8**, 22696-22704.